UNIVERSITÀ DEGLI STUDI DI GENOVA

Dottorato di Ricerca
BIOTECNOLOGIE IN MEDICINA
TRASLAZIONALE
XXXII Ciclo
Curriculum BIOIMAGING

Tesi di Dottorato

Interplay between spinal cord and cerebral
cortex metabolism in amyotrophic
lateral sclerosis

Dott. Alessandro Bellini

Tutor: Prof. Gianmario Sambuceti
Coordinatore: Prof. Rodolfo Quarto

Index

1 Figure Index

2 Table Index

3 About ALS

Amyotrophic lateral sclerosis (ALS) is a group of rare neurological diseases that mainly involve the nerve cells (neurons) responsible for controlling voluntary muscle movement. The disease is progressive, and currently there is no cure for ALS and no effective treatment to halt, or reverse, the progression of the disease.

ALS belongs to a wider group of disorders known as motor neuron diseases, which are caused by gradual degeneration and death of motor neurons. Motor neurons are nerve cells that extend from the brain to the spinal cord and to muscles throughout the body. These motor neurons initiate and provide vital communication links between the brain and the voluntary muscles.

Messages from motor neurons in the brain (called upper motor neurons) are transmitted to motor neurons in the spinal cord and to motor nuclei of brain (called lower motor neurons) and from the spinal cord and motor nuclei of brain to a particular muscle or muscles.

In ALS, both the upper motor neurons and the lower motor neurons degenerate or die, and stop sending messages to the muscles. Unable to function, the muscles gradually weaken, start to twitch (called fasciculations), and waste away (atrophy). Eventually, the brain loses its ability to initiate and control voluntary movements.

Early symptoms of ALS usually include muscle weakness or stiffness. Gradually all muscles under voluntary control are affected, and individuals lose their strength and the ability to speak, eat, move, and even breathe.

Most people with ALS die from respiratory failure, usually within 3 to 5 years from when the symptoms first appear. However, about 10 percent of people with ALS survive for 10 or more years.

The onset of ALS can be so subtle that the symptoms are overlooked but gradually these symptoms develop into more obvious weakness or atrophy that may cause a physician to suspect ALS. Some of the early symptoms include:
- fasciculations (muscle twitches) in the arm, leg, shoulder, or tongue
- muscle cramps
- tight and stiff muscles (spasticity)
- muscle weakness affecting an arm, a leg, neck or diaphragm.
- slurred and nasal speech
- difficulty chewing or swallowing.

For many individuals the first sign of ALS may appear in the hand or arm as they experience difficulty with simple tasks such as buttoning a shirt, writing, or turning a key in a lock. In other cases, symptoms initially affect one of the legs, and people experience awkwardness when walking or running or they notice that they are tripping or

stumbling more often.

When symptoms begin in the arms or legs, it is referred to as "limb onset" ALS. Other individuals first notice speech or swallowing problems, termed "bulbar onset" ALS.

No one test can provide a definitive diagnosis of ALS. ALS is primarily diagnosed based on detailed history of the symptoms and signs observed by a physician during physical examination along with a series of tests to rule out other mimicking diseases. However, the presence of upper and lower motor neuron symptoms strongly suggests the presence of the disease.

Physicians will review an individual's full medical history and conduct a neurologic examination at regular intervals to assess whether symptoms such as muscle weakness, atrophy of muscles, and spasticity are getting progressively worse.

ALS symptoms in the early stages of the disease can be similar to those of a wide variety of other, more treatable diseases or disorders.

The cause of ALS is not known, and scientists do not yet know why ALS strikes some people and not others. However, evidence from scientific studies suggests that both genetics and environment play a role in the development of ALS.

No cure has yet been found for ALS. However, there are treatments available that can help control symptoms, prevent unnecessary complications, and make living with the disease easier.

4 Introduction

As mentioned, ALS is a neurodegenerative disorder, characterized by a degeneration of upper and lower motor neurons leading to a progressive muscular paralysis. Although median survival most often averages 3–5 years, the large variability of its course (Calvo *et al.*, 2017 [7]) raises an urgent need to develop biomarkers able to characterize the mechanisms underlying disease progression and to improve the diagnostic yield of clinical and neuro-physiological evaluation.

Most studies in this setting focused on cortical response to ALS. Among these approaches, brain PET studies with ^{18}F-fluorodeoxyglucose (FDG) already reported a significant reduction in glucose metabolism (Pagani *et al.*, 2014 [30]) in motor and premotor cortex (Kiernan *et al.*, 1994 [15]; Abrahams *et al.*, 1996 [1], 2005 [2]). By contrast, involvement of the spinal cord has been characterized in relatively lower detail, mostly because of the anatomical features of this structure that limit the standardization of its evaluation. Consequently, a large uncertainty still exists about the mechanisms underlying ALS-induced damage in the spinal cord and its relationship with cortical impairment. We recently reported the potential of the Hough transform in delineating spinal cord structure and metabolic activity in a population of ALS patients subjected to FDG PET/CT (Marini *et al.*, 2016 [23]). Specifically, this classical pattern recognition approach for the automatic identification of straight lines in the image has been recently extended to the recognition of more complex shapes. This computational 3D approach enabled the extraction of spinal cord metabolic information from whole body images and permitted us to document increased glucose consumption, possibly representing a potential and independent prognostic marker (Marini *et al.*, 2016 [23]).

In the present study, we simultaneously analysed brain and spinal cord FDG uptake in a series of prospectively recruited patients submitted to brain and wholebody PET/CT.

5 Materials and methods

5.1 Patients with amyotrophic lateral sclerosis

The study included 44 prospectively recruited patients with definite, probable or probable laboratory-supported ALS diagnosis according to the revised El-Escorial criteria (Brooks *et al.*, 2000 [6]). None of them had any history of other neurological disorders, cerebrovascular disease, diabetes mellitus or systemic inflammatory disease. All subjects provided signed informed consent to enter the study that was approved by the Ethics Committees of IRCCS Ospedale Policlinico San Martino in Genoa, and of AUO Città della Salute e della Scienza in Turin, Italy.

5.2 Control subjects

Brain PET from patients with ALS were compared with the corresponding data of 44 healthy volunteers who gave their informed consent. As described by Morbelli et al. (2017 [26]), their healthy condition was carefully checked by means of clinical and neuropsychological examination, brain MRI and by the same exclusion criteria as used for ALS patients. A case–control criterion was adopted to reproduce the same age range, gender distribution and educational level of ALS patients.

For ethical considerations, PET/CT scan was not extended to the body of these normal volunteers. Accordingly, PET spinal cord data were compared with the corresponding findings of 44 control subjects without any history of neurodegenerative disease, randomly selected from a previously published normalcy database (Sambuceti et al., 2012 [33]), again according to a case–control criterion.

5.3 PET/CT imaging

All PET/CT scans were acquired according to current guidelines (Varrone *et al.*, 2009 [35])

All subjects were studied in the early morning after ≥6 h fasting. Serum glucose was assessed, and an antecubital vein was cannulated. According to current guidelines (Hoffman et al., 1992 [13]), patients were invited to lye for 20 min in a silent and darkened room, with eyes closed and ears unplugged. A bolus of FDG (4.8-5.2 MBq/kg body weight) was then injected 45-60 minutes before 3D-scan using an integrated PET/CT scanner (Hirez 16, Siemens Medical Solutions or Discovery GE Healthcare, depending on the centre). In all cases, the 15 minutes cerebral acquisition was followed by whole body imaging in arms down position.

In both centers, PET data were reconstructed into a 128×128 matrix using a 3D iterative reconstruction algorithm (ordered-subsets

expectation maximization, three iterative steps, eight subsets). Raw images were scatter-corrected and processed using a 3D Gaussian filter, while CT was used for attenuation correction.

Image quality control documented a spatial resolution of 4.0 mm full-width at half-maximum for both scanners. According to standard procedures of both labs, the two imaging systems were cross-calibrated using a cylinder of 20 cm diameter and 20 cm length filled with a solution containing 100 MBq of 18F-FDG that was counted for 1 h to minimize the statistical noise, and images were reconstructed with the same algorithm used for the clinical protocol.

5.4 Spinal cord analysis

The entire CT dataset was co-registered with the 3D PET images using commercially available software interfaces.

Image analysis was performed by means of a pattern recognition algorithm based on an extension of the Hough transform to algebraic curve. This approach uses an operator-independent fully deterministic algorithm to identify the spinal canal and to extract spinal cord FDG uptake expressed as standardized uptake value (SUV)

The computational method has been previously described by Ricca et al. (2016 [31]).

It was first observed that spinal cord profile is reliably approximated by an ellipse. Let $p = (x_p, y_p)$ be a point in the image plane satisfying the equation of the ellipse

$$\mathcal{C}_{a,b} : \frac{x^2}{a^2} + \frac{y^2}{b^2} = 1$$

Then, the Hough transform of p with respect to the family of curves $\mathcal{F} = \left\{ \mathcal{C}_{a,b} \right\}$, is the curve $\Gamma_p(\mathcal{F})$ of equation

$$\Gamma_p(\mathcal{F}) : B^2 x_p^2 + A^2 y_p^2 = A^2 B^2$$

in the parameter space $\langle A, B \rangle$ where the two real, positive, and independent parameters a, b vary. The Hough transform method relies on the mathematical fact that when p varies on $\mathcal{C}_{a,b}$ then all curves $\Gamma_p(\mathcal{F})$ intersect in exactly one point in the parameter space. From a computational viewpoint this fact naturally inspires a pattern recognition method according to which the parameter space is discretized in cells, an accumulator function is defined on it, and the ellipse in the image space is identified by the parameters providing the maximum of such function. This method can be extended to the

recognition of a vast class of algebraic curves in the image space.

Moreover, Beltrametti et al. (2013 [5]) showed that the method is robust with respect to both image noise and spatial inaccuracy in the image. Finally, the Hough transform technique shows a better sensitivity with respect to standard gradient-based methods, since it behaves reliably even in the case of low contrast.

We applied this scheme to the recognition of both the spinal canal and the spinal cord districts in whole-body CT images of control subjects and ALS patients. Specifically, the family of curves with three convexities, represented by the equation

$$C_{a,b}: (x^2 + y^2)^3 = \left(a(x^2 + y^2) - b(x^3 - 3xy^2)\right)^2$$

was particularly appropriate for the optimal detection of the spinal canal (Figure 1).

By contrast, the four-parameter family of ellipses expressed in the form

$$E_{a,b,c,d}: b^2(x - c)^2 + a^2(y - d)^2 - a^2b^2 = 0$$

was the best candidate for identifying the spinal cord district.

For each CT slice, the two curves identifying the spinal canal and SC were used to create two sets of binary masks with one zero outside and one inside each curve, respectively. These masks were multiplied against the co-registered PET slice in order to digitally extract the metabolic information represented as standardized uptake value (SUV) of local FDG radioactivity

The different spinal canal and spinal cord districts were defined anatomically considering the cervical segment as the region between the skull base and the plane adjacent to the caudal face of the C7 vertebral body. The dorsal segment was defined as the district between this plane and the one adjacent to the caudal face of D12. The sacral and lumbar canal districts were *a priori* excluded since considered free from spinal cord.
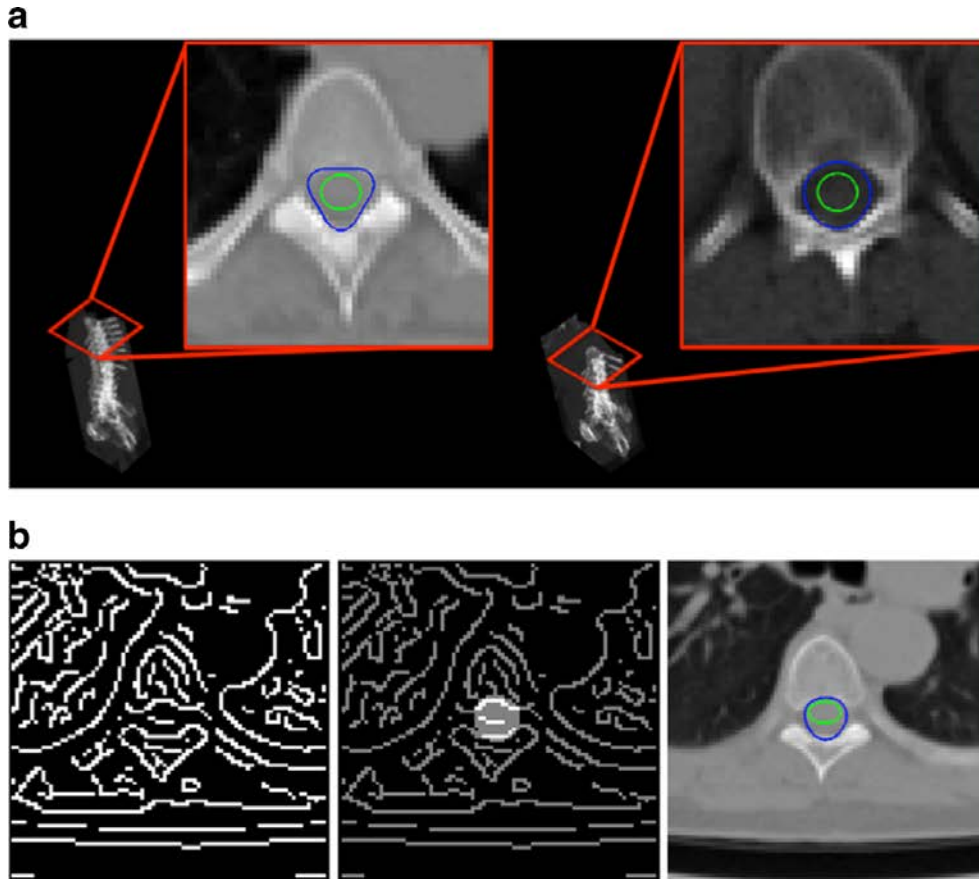
Figure 1: (a) Detection of spinal canal and spinal cord at different heights of the vertebral column. The Hough transform-based procedure with respect to the curve with three convexities allows identification of the spinal canal (*blue line*), while the spinal cord is detected by the Hough transform-based procedure with respect to the ellipse (*green line*). **(b)** *Left to right*: edge detection of a CT slice in the vertebral region; edge points inside the region bounded by the curve with three convexities; and the curve with three convexities (*blue line*) and the ellipse (*green line*) detected by applying the Hough transform-based procedure.

5.5 Brain PET analysis

Statistical Parametric Mapping (SPM) analysis was performed as previously described (Morbelli *et al.*, 2017 [26]).

Original DICOM images were converted to NifTI-1 format using SPM8 DICOM Import (Varrone et al., 2009 [35]). PET images were normalized to a customized previously published template (Della Rosa et al., 2014 [10]) and smoothed with 8-mm full width at half maximum Gaussian Kernel. Subsequently, tracer distribution was scaled for whole brain radioactivity concentration to identify areas of relative hypo- or hypermetabolism in ALS group by means of a two-sample t test. The same algorithm was used to analyze FDG distribution within ALS group according to either disease presentation (bulbar or spinal) and side involvement at diagnosis. Finally, multiple regression analysis was performed to identify areas whose metabolism was directly o inversely correlated with SC SUV.

This analysis was performed without any a priori definition, considering SC SUV as covariate. Age, gender and center of belonging were included as nuisance in all SPM analyses with significance threshold set at p<0.05, False-Discovery-Rate (FDR)-corrected both at peak and at cluster level. Only significant clusters containing at least 100 voxels were taken into consideration. BrainMap GingerALE 2.3 (Eickhoff SB, Laird AR.) was used to convert coordinates of significant clusters in Montreal Neurological Institute space into Talairach coordinates. Brodmann areas (BAs) were then identified at a range of 0 to 3 mm from the corrected Talairach coordinates of the SPM output isocenters, after importing the corrected coordinates by means of Talairach client (http://www.talairach.org/index.html).

To compare ALS effects on global consumption of brain and spinal cord, SPM analysis of FDG uptake distribution was complemented with the evaluation of absolute tracer retention. Accordingly, the preprocessed NifTI-1 PET images were converted in whole-brain SUV parametric maps dividing the product between radiotracer concentration (kBq/ml) and body weight (in kg) by the injected FDG dose (in MBq) (Cistaro et al., 2012 [8]; Ku̇ntzelmann et al., 2013 [17]; Annen et al., 2016 [3]).

Thereafter, we automatically identify volumes of interest corresponding to 41 Brodmann areas (BAs) in both hemispheres. Our Volumes Of Interest (VOIs) masks were created using WFU PickAtlas (Lancaster et al., 1997 [18], 2000 [19]) and we used NiftyReg (TIG, Translational Imaging Group) to register the Atlas's reference image on each patient's PET; using these transformations we were able to register each mask on the corresponding PET, in order to extract PET signal (SUV) from each VOI.

All data are reported as mean ± standard deviation (SD). Unpaired or paired t-tests were used, as appropriate. P-values < 0.05 were considered significant. Analyses were performed using SPSS package (version 21).

6 Results

6.1 Clinical characteristics of patient population

As reported in Table 1, age, sex, and ideal body weight were similar in control and ALS subjects. ALS Functional Rating Scale Revised (ALSFRS-R) score, updated at imaging date, was 39 ± 4 (range 28–45). Mean time elapsed from clinical disease onset and PET/CT scanning was 20 ± 15 months (range 8–81 months, median 14 months) while mean interval between ALS diagnosis and imaging was 10 ± 9 months.

Table 1: Demographic of patients population

Number	44
Age (years)	64±10
Men	25
Women	19
Spinal onset	35 (80%)
Bulbar onset	9 (20%)
Right sided	16/35
Left sided	14/35
Bilateral	5/35
Upper limb onset	12 / 35
Lower limb onset	21 / 35
Combined limbs onset	2 / 35
Time elapsed from ALS diagnosis and PET/CT imaging (months)	10±9
ALS functional rating scale	39±5

6.2 Spinal cord metabolism

FDG uptake was significantly higher in the whole spinal cord of ALS patients with respect to controls (0.81 ± 0.4 versus 0.67 ± 0.2, $P = 0.05$). This difference was more pronounced in cervical segments (1.08 ± 0.2 versus 0.82 ± 0.2, $P < 0.01$) and relatively less evident in dorsal metameres (0.69 ± 0.2 versus 0.57 ± 0.2, $P < 0.05$). Effect of ALS on spinal cord metabolism was independent from demographic and clinical variables as well as from time elapsed from diagnosis to imaging. Likewise, spinal cord metabolic activation was similar in spinal or bulbar onset ALS. Yet, the regional agreement between increased FDG uptake and

clinical motor impairment could be documented in the 33/35 spinal patients in whom predominantly upper ($n = 12$) or lower ($n = 21$) limb involvement was well defined at diagnosis (Figure 2). Upper limb onset was associated with a more pronounced metabolic activation in the cervical segment (Figure 2). The selectivity of this metabolic response was confirmed by the ratio between cervical and dorso-lumbar spinal cord tracer retention that was significantly higher in patients with upper limb.
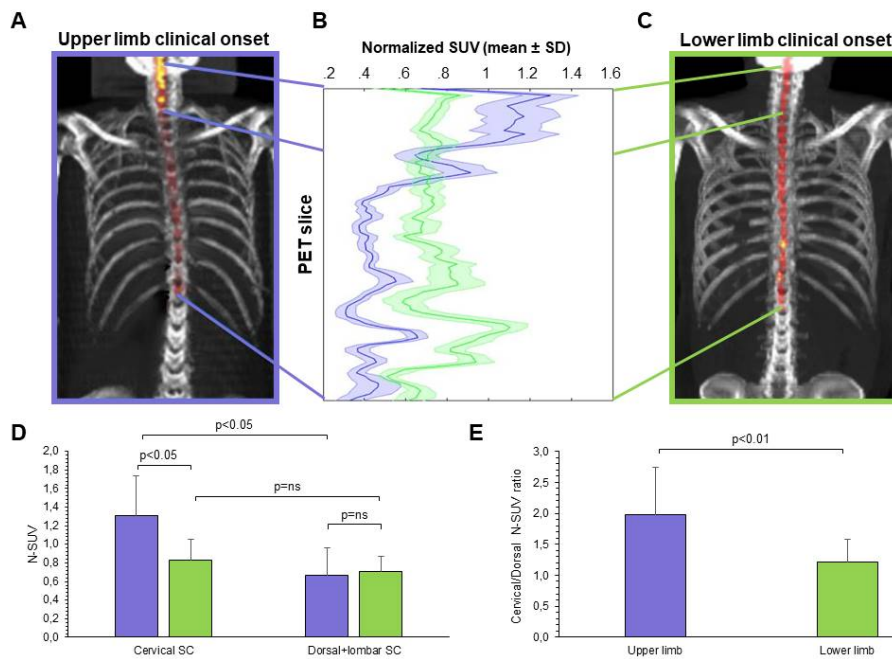
Figure 2: Panels A and C display two 3D reconstructions of SC FDG uptake, in a patient with upper or lower ALS onset, respectively. B panel reports the corresponding SUV values plotted from cervical slices (top) to lumbar ones (bottom). Tracer retention is higher in cervical segments in upper limb presentation, while the reverse gradient occurs in lower limb onset. Panel D displays average SUV values in the two SC districts: in patients with upper limb onset tracer uptake in the cervical SC is higher with respect to both the dorsal segment in the same patients and with respect to the same segment in the remaining subjects. This selective localization is confirmed by the ratio cervical/dorso-lumbar tracer uptake reported in panel E.

6.3 SPM analysis of amyotrophic lateral sclerosis effect on brain FDG distribution

SPM-based group analysis highlighted a wide hypometabolic cluster involving frontal dorso-lateral cortex bilaterally as well as the precentral and temporal cortex in the left hemisphere (Figure 3A and Table 2). Conversely, hypermetabolic cluster was markedly smaller and mainly involved the midbrain (Figure 3B and Table 2). This metabolic pattern was reproduced in spinal as well as in bulbar onset patients. Bulbar onset was instead associated with a more severe metabolic impairment in bilateral precentral gyri (BA 6) and in left putamen (Figure 4 and Table 3).

Among the 35 patients with spinal ALS, right onset was associated with a more severe metabolic impairment in the left premotor cortex (BA 6) and in the left temporal cortex (BA 39) as well as in the right postcentral gyrus (BA 3) (Figure 5 and Table 4). By contrast, no appreciable difference in brain metabolism was identified between ALS patients classified according to upper or lower limb clinical onset.

Mean SUV of cervical spinal cord was significantly and inversely correlated with hypometabolism in the pre- and para-central gyri bilaterally but particularly in the left hemisphere (Figure 3C and Table 2). Similarly, dorsal spinal cord mean SUV predicted a relative hypometabolism in the temporo-lateral and frontal dorso-lateral cortex in the left hemisphere (Figure 3D and Table 2). Finally, neither cervical nor dorsal spinal cord metabolism were significantly correlated with midbrain metabolic pattern.
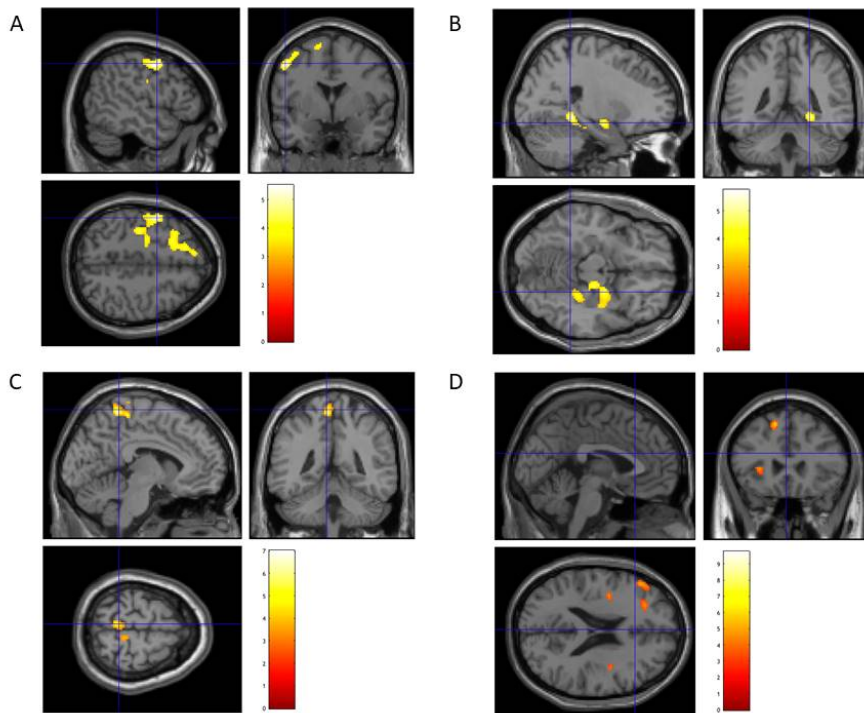
Figure 3: SPM analysis. 3D rendering showing regions in which FDG uptake was significantly lower (A) or higher (B) in ALS patients with respect to controls. (C and D) Results of the multiple regression analysis between brain and cervical or dorsal spinal cord metabolism, respectively. Threshold P<0.05, corrected for multiple comparisons with the FDR at the voxel level were set in each analysis. Coordinate and regional details are presented in Table 1.

Table 2: SPM analysis

Cluster Extent	Corrected P-value	Cortical region	Maximum Z-score	Talairach Coordinates x, y, z	Cortical region	BA
				Cluster level / Peak level		

| Cluster Extent	Corrected P-value	Cortical region	Maximu Z-score	Talairach Coordinates x, y, z	Cortical region	BA
— Cortical regions of relative hypometabolism						
1357	0.0001	L-limbic	5.48	–33 –9 –34	Uncus	20
		L-limbic	5.35	–36 –18 –26	Uncus	20
		L-temporal	4.78	–45 –22 –21	Fusiform gyrus	20
1619	0.0001	L-frontal	5.06	–49 1 45	Middle frontal gyrus	6
		L-frontal	4.97	–32 15 51	Superior frontal	8
		R-frontal	4.58	15 30 49	Superior frontal	8
— Cortical regions of relative hypermetabolism						
384	0.01	R-frontal	5.19	11 –19 –13	Superior frontal	8
		R-sublobar	4.74	23 –8 –8	Amygdala	
		R-sublobar	3.83	13 –2 0	Lentiform nucleus	
		R-sublobar	3.50	36 –9 16	Insula	13
379	0.01	R-midbrain	4.69	7 –18 –19		
— Correlation between cervical spinal cord and brain metabolism						
349	0.01	L-frontal	4.13	–5 –40 57	Paracentral lobule	5
		R-frontal	4.11	15 -24 69	Precentral gyrus	4
		L-frontal	3.62	–5 -30 56	Paracentral lobule	6
— Correlation between dorsal spinal cord and brain metabolism						
409	0.01	R-sublobar	4.75	42 –7 16	Insula	13
		R-sublobar	3.55	41 4 12	Insula	13
		R-sublobar	3.39	34 -14 15	Claustrum	
347	0.01	L-frontal	4.46	-13 23 49	Superior frontal	6
		L-limbic	3.79	–7 17 37	Cingulate gyrus	32
		L-limbic	3.48	–5 0 42	Cingulate gyrus	24
590	0.01	L-sublobar	4.07	–34 –9 15	Insula	13
		L-sublobar	3.49	–36 –2 23	Insula	13
		L-frontal	3.30	-41 6 36	Precentral gyrus	9
436	0.01	L-frontal	3.55	-49 35 18	Middle frontal gyrus	
		L-frontal	3.16	-25 34 21	Medial frontal gyrus	9
		L-frontal	3.14	-31 30 32	Middle frontal gyrus	9
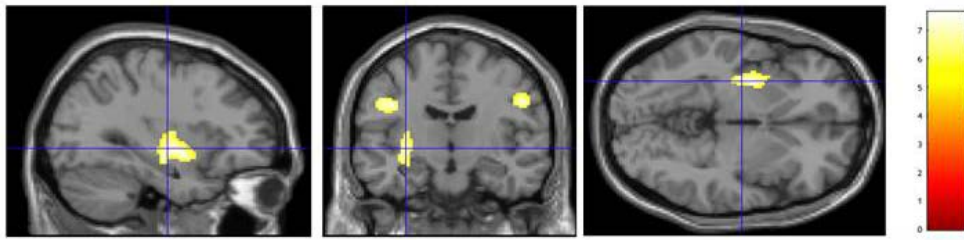
Figure 4: Topographic localization of hypometabolic clusters in bulbar versus spinal ALS. SPM analysis was performed with threshold set at p<0.05, FWE corrected. Cluster, extension and localization is also described in the Table 3.

Table 3: SPM analysis in bulbar versus spinal ALS

| Cluster Extent | Cluster Level | | Peak Level | Talairach Coordinates | | | Cortical Region | BA |
	corrected P value	Cortical region	Maximum Z score	x, y, z				
547	0.0001	L-Sub Lobar	5.75	-29	-4	-1	Putamen	
		L-Sub Lobar	5.57	-31	-12	0	Putamen	
		L-Frontal	5.25	-22	6	-11	Subcallosal Gyrus	34
		L-Frontal	5.66	-37	-13	29	Precentral Gyrus	6
131	0.0001	R-Frontal	5.53	50	-9	31	Precentral Gyrus	6
131	0.0001	R-Frontal	4.98	41	-12	40	Precentral Gyrus	6
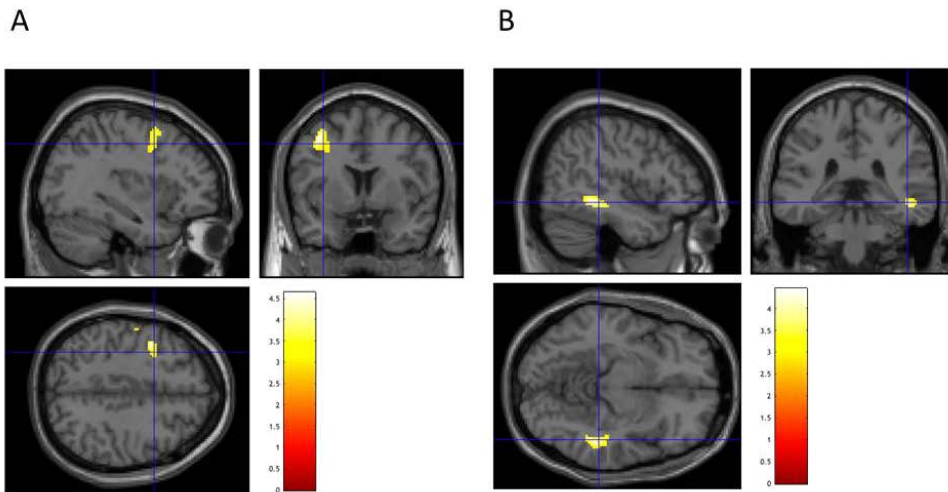
Figure 5: Comparison between right and left ALS clinical onset. Cluster were regarded as significant if they survived at p<0.005, no FWE corrected. SPM analysis was performed with threshold set at p<0.005 no FWE corrected. Panel A shows the topographic representation of clusters in which FDG uptake was significantly lower in right than in left clinical onset ALS patients. Panel B represents the clusters in which FDG uptake was significantly lower in left than in right clinical onset ALS patients. Cluster extension and localization are also described in Table 4.

18

Table 4: SPM analysis in left and right clinical onset

Cluster Extent	Cluster Level corrected P value	Cortical region	Peak Level Maximum Z score	Talairach Coordinates			Cortical Region	BA
				Left < Right				
286	0.022	L-Temporal	3.77	-49	-63	11	Middle Temporal Gyrus	39
		L-Temporal	3.57	-56	-68	25	Middle Temporal Gyrus	39
225	0.038	L-Limbic	3.70	-19	-57	6	Posterior Cingulate	30
204	0.047	R-Frontal	3.69	32	-25	65	Precentral Gyrus	4
		R-Parietal	3.15	45	-25	60	Postcentral Gyrus	3
		R-Parietal	3.00	41	-31	46	Inferior Parietal Lobule	40
173	0.064	L-Frontal	3.68	-37	7	44	Middle Frontal Gyrus	6
145	0.087	L-Frontal	3.37	-54	-7	34	Precentral Gyrus	6
		L-Frontal	2.85	-43	-11	31	Precentral Gyrus	6
				Right < Left				
154	0.079	R-Temporal	3.66	44	-44	-2	Sub-Gyral	37

6.4 Volumes of interest analysis

FDG uptake, estimated by average SUV of automatically identified volumes of interest, was significantly lower in ALS patients with respect to controls in virtually all analysed BAs (Figure 6). As a consequence, this same observation also applied when the average SUV of the whole cortical volume was considered (4.93 ± 1.40 versus 5.95 ± 1.65, respectively, $P < 0.01$). Similarly, ALS was associated with lower SUV in thalamus (5.31 ± 1.76 versus 6.4 ± 1.7, respectively, $P<0.01$), basal ganglia (6.17 ± 1.75 versus 7.2 ± 2.0, respectively, $P<0.01$) and cerebellum (3.1 ± 1.98 versus 5.6 ± 1.5, respectively, $P<0.01$).
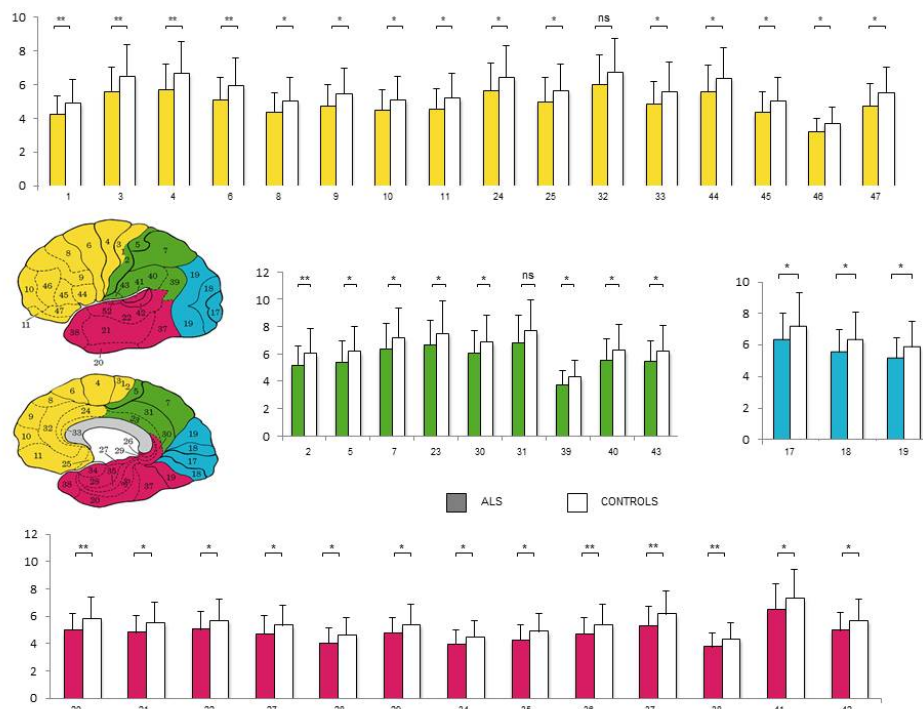

Figure 6: Volumes of interest analysis. BA SUV values in ALS (filled bars) and control subjects (open bars) according to cortical lobes. The y-axes represent BA SUV values. Yellow = frontal lobe; green = parietal lobe; blue = occipital lobe; pink = temporal lobe. *P<0.05; **P<0.01

7 Discussion

The main finding of the present study is the divergent metabolic response to ALS in brain and spinal cord. Brain displays a generalized reduction in glucose consumption particularly evident in motor and premotor cortex. By contrast, spinal cord displays a moderate increase in FDG uptake that can be more easily detected in its cervical segment. The interplay between the two opposite metabolic patterns, documented by this transversal and simultaneous picture, indicates a divergent nature or a divergent time-course of the mechanisms underlying ALS-related damage to upper and lower motor neurons.

In agreement with our previous observation (Marini *et al.*, 2016 [23]), the analysis of spinal cord metabolic pattern showed a significant increase in FDG uptake in the spinal cord of ALS patients. The reproducibility of this finding and its occurrence in a cohort of prospectively and independently recruited ALS subjects confirm that 'metabolic spinal cord activation' might occur in a high number of ALS patients and might thus track pathophysiological mechanisms potentially contributing to disease progression. This concept is corroborated by the observation that, among spinal onset ALS patients, upper limb presentation was associated with a more pronounced metabolic activation of cervical spinal cord. This finding thus suggests that spinal cord metabolic activation might track some process related to motor impairment on a regional basis. Actually, the opposite pattern was not observed in patients with lower limb involvement most likely because of the limited spatial resolution hampering the evaluation of caudal spinal cord because of contaminations related to both partial volume effect and uncertainty in the definition of caudal spinal cord border.

On the other hand, SPM analysis of brain FDG distribution confirmed previous studies in larger numbers of patients reporting small areas of relative hypermetabolism virtually limited to the midbrain and large hypometabolic clusters in the frontal dorso-lateral cortex (Cistaro *et al.*, 2012 [8]; Pagani *et al.*, 2014 [30]) with the uncus involved only in our series.

Bulbar phenotype was characterized by a more pronounced metabolic impairment in bilateral pre-central gyri and in left putamen. This finding agrees with data by Kim et al. [16] who reported that the putamen was among the most atrophied brain regions in cognitively impaired ALS patients. On the other hand, the finding of a relatively reduced bilateral frontal metabolism supports the growing evidence of cognitive and extramotor changes in bulbar pathology and seems to confirm the divergent neuropsychological and functional patterns in bulbar and spinal onset ALS.

Right onset ALS was associated with a more severe metabolic impairment in the left hemisphere at SPM analysis. However, this finding has to be cautiously interpreted due to the possible occurrence of several biases related to the limited sample size and the variable side with most prominent symptoms at time of scan.

Accordingly, the simultaneous coupling of both evaluations provided a new and, under many points of view, unexpected glance at available data about ALS metabolic effect on the CNS (central nervous system).

Currently, SPM is one of the most widely used standards to evaluate brain FDG images. In conventional 'static' PET studies, this procedure analyses the original reconstructed data reporting radioactivity concentration (in kBq/ml) in each voxel. These source images are thus scaled to an intracranial reference region to identify areas of relative activation (hypermetabolism) or stilling (hypometabolism). However, scaling procedure intrinsically prevents the capability to identify generalized reductions in brain glucose consumption. Indeed, several authors argued about the interpretation of voxelwise-highlighted hypermetabolic clusters that might reflect a true metabolic activation as well a relatively less severe metabolic deceleration in neurodegenerative disorders (Ku̇ntzelmann et al., 2013 [17]).

To overcome this limitation, and to replicate the analysis criteria adopted for spinal cord evaluation, we processed the original data of tracer concentration to calculate average SUV in each automatically detected volume of interest. Obviously, this procedure does not account for both FDG persistence in the circulating blood and competition by serum glucose level. Nevertheless, its capability to abolish the interference of the main methodological determinants of tracer uptake administered dose and body weight permitted us to detect a generalized reduction of FDG uptake in studied ALS patients.

This finding confirms previous dynamic PET studies that reported a generalized and progressive reduction of glucose consumption in ALS brain partially related to disease duration (Dalakas et al., 1987 [9]), degree of cognitive decline (Ludolph et al., 1992 [22]) or severity of upper motor neuron involvement (Hoffman et al., 1992 [13]). Similarly, localization of metabolic impairment, provided by voxelwise analysis, closely agrees with the thinning of the primary motor cortex previously documented by MRI in ALS patients (Verstraete et al., 2010 [36]) and also with recent (Eisen et al., 2017 [11]) and older neuropathological studies reporting abnormalities not only in the Betz area (Lawyer et al., 1953 [20]) but also in the adjacent gyri and in the deeper parts of the brain (Smith et al., 1960

[34]). Unfortunately, the lack of coregistered PET and MRI images prevents the possibility to define whether the reduced tracer uptake in hypometabolic areas reflects a reduced density of cells with an intact metabolism, a reduced metabolic rate of glucose consumption by normal populations of synapses or both mechanisms. Nevertheless, the same analytical approach documented that the metabolic activation of spinal cord faced a global impairment in glucose consumption involving the vast majority of encephalic structures.

The mechanisms underlying this opposite response cannot be identified by the present data. Nevertheless, post-mortem studies document the activation of microglia (Beers et al., 2006 [4]), oligodendrocytes (Lee et al., 2012 [21]) and astrocytes (Nagai et al., 2007 [28]) in tissues harvested from motor cortex and spinal cord of both ALS patients and experimental models of ALS. In particular, astrocytic activation nicely fits with the notion that these cells account for most of the FDG accumulation in the brain (Zimmer et al., 2017 [37]). Defining these mechanisms is obviously far beyond the scope of this clinical and observational study. Nevertheless, the divergent pattern of FDG uptake in the spinal cord and brain indicates that the metabolic response of these two districts follows different pathways or different time sequences. Accordingly, monitoring the temporal evolution of damage in the first and in the second motor neuron might represent an important clue to improve our understanding of ALS pathophysiology. Obviously, a direct estimation of brain glucose consumption would have provided a more detailed description of metabolic pattern in both brain and spinal cord (Hustinx et al., 1999 [14]). Ethical concerns prevented the possibility to perform a complex series of acquisitions with dynamic sequence followed by brain and whole-body scans. Nevertheless, the decreased FDG uptake in the brain, together with the opposite response of spinal cord SUV, strongly support the concept that hypermetabolic brain clusters identified by SPM analysis probably reflect areas of relatively preserved glucose consumption rather than the consequence of neuronal activation (Pagani et al., 2014 [30]).

As a main limitation of our study, brain and spinal cord metabolic patterns of ALS patients were compared with normalcy databases harvested from different populations. In brain-image donors, this limitation was justified by the ethical concern in extending CT scan to the whole body of normal volunteers. For normal spinal cord evaluation, the ethical concern was related to the need to avoid modifications to the standard protocol of oncologic imaging that does not include the pre-scan procedure needed for cerebral PET/CT. As a further limitation, the limited patient sample and the relatively wide

inclusion criteria did not permit us to verify any possible correlation between degree/site of spinal cord metabolic activation and force generated by the related muscular districts. A similar consideration applies to the side coherence between brain metabolism and motor involvement. Actually, when compared with left onset, right onset ALS was associated with a more severe metabolic impairment in the left hemisphere.

However, this finding must be interpreted cautiously because of the possible occurrence of several biases related to the limited sample size and the variable side with most prominent symptoms at time of scan.

In conclusion, the present transversal and observational study documents a divergent metabolic response to ALS by spinal cord and brain. This evidence indicates that whatever mechanism affects glucose consumption of the CNS in ALS, its nature or its time course profoundly differ in upper and lower motor neurons. This divergent behaviour indicates that complementing brain imaging with the extraction of spinal cord information might improve the informative potential of PET studies with tracers selectively interrogating specific pathophysiological mechanisms underlying ALS progression.

8 References

1. Abrahams S, Goldstein LH, Kew JJ, Brooks DJ, Lloyd CM, Frith CD, et al. Frontal lobe dysfunction in amyotrophic lateral sclerosis: a PET study. Brain 1996; 119: 2105–20.

2. Abrahams S, Goldstein LH, Suckling J, Ng V, Simmons A, Chitnis X, et al. Frontotemporal white matter changes in amyotrophic lateral sclerosis. J Neurol 2005; 252: 321–31.

3. Annen J, Heine L, Ziegler E, Frasso G, Bahri M, Di Perri C, et al. Function-structure connectivity in patients with severe brain injury as measured by MRI-DWI and FDG-PET. Hum Brain Mapp 2016; 37: 3707–20.

4. Beers DR, Henkel JS, Xiao Q, Zhao W, Wang J, Yen AA, et al. Wild-type microglia extend survival in PU.1 knockout mice with familial amyotrophic lateral sclerosis. Proc Natl Acad Sci USA 2006; 103: 16021–6.

5. Beltrametti MC, Massone AM, Piana M. Hough transform of special classes of curves. SIAM J Imaging Sci 2013; 6: 391–412.

6. Brooks BR, Miller RG, Swash M, Munsat TL. El Escorial revisited: revised criteria for the diagnosis of amyotrophic lateral sclerosis, Amyotroph Lateral Scler Other Motor Neuron Disord 2000; 1: 293–99.

7. Calvo A, Moglia C, Lunetta C, Marinou K, Ticozzi N, Ferrante GD, et al. Factors predicting survival in ALS: a multicenter Italian study. J Neurol 2017; 264: 54–63.

8. Cistaro A, Valentini MC, Chiò A, Nobili F, Calvo A, Moglia C, et al. Brain hypermetabolism in amyotrophic lateral sclerosis: a FDG PET study in ALS of spinal and bulbar onset. Eur J Nucl Med Mol Imaging 2012; 39: 552.

9. Dalakas MC, Hatazawa J, Brooks RA, Di Chiro G. Lowered cerebral glucose utilization in amyotrophic lateral sclerosis. Ann Neurol 1987; 22: 580–6.

10. Della Rosa PA, Cerami C, Gallivanone F, Prestia A, Caroli A, Castiglioni I, Gilardi MC, Frisoni G, Friston K, Ashburner J, Perani D; EADC-PET Consortium. A standardized [18F]-FDG-PET template for spatial normalization in statistical parametric mapping of dementia. Neuroinformatics. 2014 Oct;12(4):575-93. doi: 10.1007/s12021-014-9235-a

11. Eisen A, Braak H, Del Tredici K, Lemon R, Ludolph AC, Kiernan MC. Cortical influences drive amyotrophic lateral sclerosis. J Neurol Neurosurg Psychiatry 2017; 88: 917–24.

12. Friston KJ, Frith CD, Liddle PF, Frackowiak RS. Functional connectivity: the principal-component analysis of large (PET) data sets. J Cereb Blood Flow Metab. 1993;13:5-14

13. Hoffman JM, Mazziotta JC, Hawk TC, Sumida R. Cerebral glucose utilization in motor neuron disease. Arch Neurol 1992; 49: 849–54

14. Hustinx R, Smith RJ, Benard F, Bhatnagar A, Alavi A. Can the standardized uptake value characterize primary brain tumors on FDG-PET? Eur J Nucl Med 1999; 26: 1501–9.

15. Kiernan JA, Hudson AJ. Frontal lobe atrophy in motor neuron dis- eases. Brain 1994; 117: 747–57.

16. Kim HJ, Oh SI, de Leon M, Wang X, Oh KW, Park JS, et al. Structural explanation of poor prognosis of amyotrophic lateral sclerosis in the nondemented state. Eur J Neurol. 2016;24:122-9.

17. Kün̈tzelmann A, Guenther T, Haberkorn U, Essig M, Giesel F, Henze R, et al. Impaired cerebral glucose metabolism in prodromal Alzheimer's disease differs by regional intensity normalization. Neurosci Lett 2013; 534: 12–7.

18. Lancaster, J.L., Summerln, J.L., Rainey, L., Freitas, C.S., Fox, P.T., 1997. he Talairach Daemon, a database server for Talairach Atlas Labels. NeuroImage 5, S633.

19. Lancaster, J.L., Woldorff, M.G., Parsons, L.M., Liotti, M., Freitas, C.S., Rainey, L., Kochunov, P.V., Nickerson, D., Mikiten, S.A., Fox, P.T., 2000. Automated Talairach atlas labels for functional brain mapping. Hum. Brain Mapp. 10, 120–131

20. Lawyer T, Netsky MG. Amyotrophic lateral sclerosis. A clinicoanatomic study of fifty-three cases. Arch Neurol Psychiatry 1953; 69: 171–92.

21. Lee Y, Morrison BM, Li Y, Lengacher S, Farah MH, Hoffman PN, et al. Oligodendroglia metabolically support axons and contribute to neurodegeneration. Nature 2012; 487: 443–8.

22. Ludolph AC, Langen KJ, Regard M, Herzog H, Kemper B, Kuwert T, et al. Frontal lobe function in amyotrophic lateral sclerosis: a neuropsychologic and positron emission tomography study. Acta Neurol Scand 1992; 85: 81–9.

23. Marini C, Cistaro A, Campi C, Calvo A, Caponnetto C, Nobili FM, et al. A PET/CT approach to spinal cord metabolism in amyotrophic lateral sclerosis. Eur J Nucl Med Mol Imaging 2016; 43: 2061–71.

24. Marini C, Morbelli S, Cistaro A, Campi C, Caponnetto C, Bauckneht M, Bellini A, Buschiazzo A, Calamia I, Beltrametti MC, Margotti S, Fania P, Poggi I, Cabona C, Capitanio S, Piva R, Calvo A, Moglia C, Canosa A, Massone AM, Nobili F, Mancardi G, Chio` A, Piana M, Sambuceti G. Interplay between spinal cord and cerebral cortex metabolism in amyotrophic lateral sclerosis. BRAIN 2018: 141; 2272–2279

25. Massone AM, Perasso A, Campi C, Beltrametti MC. Profile detection in medical and astronomical images by means of the Hough transform of special classes of curves. J Math Imaging Vis 2015; 51: 296–310.

26. Morbelli S, Bauckneht M, Arnaldi D, Picco A, Pardini M, Brugnolo A, et al. 18F-FDG PET diagnostic and prognostic patterns do not overlap in Alzheimer's disease (AD) patients at the mild cognitive impairment (MCI) stage. Eur J Nucl Med Mol Imaging 2017; 44: 2073–83.

27. Morbelli S, Rodriguez G, Mignone A, Altrinetti V, Brugnolo A, Piccardo A, et al. The need of appropriate brain SPECT templates for SPM comparisons. Q J Nucl Med Mol Imaging. 2008;52:89-98.

28. Nagai M, Re DB, Nagata T, Chalazonitis A, Jessell TM, Wichterle H, et al. Astrocytes expressing ALS-linked mutated SOD1 release factors selectively toxic to motor neurons. Nat Neurosci 2007; 10: 615–22.

29. NIH, National Institute of Neurological Disorders and Strokes https://www.ninds.nih.gov/

30. Pagani M, Chio` A, Valentini MC, O¨ berg J, Nobili F, Calvo A, et al. Functional pattern of brain FDG-PET in amyotrophic lateral sclerosis. Neurology 2014; 83: 1067–74.

31. Ricca G, Beltrametti M C, Massone A M. Detecting curves of symmetry in image via Hough transform. Math. Comp. Sci. 2016; 10(1): 179-205

32. Robinson JD, Lupkiewicz SM, Palenik L, Lopez LM, Ariet M. Determination of ideal body weight for drug dosage calculations. Am J Hosp Pharm. 1983;40:1016–9

33. Sambuceti G, Brignone M, Marini C, Massollo M, Fiz F, Morbelli S, et al. Estimating the whole bone-marrow asset in humans by a computational approach to integrated PET/CT imaging. Eur J Nucl Med Mol Imaging 2012; 39: 1326–38.

34. Smith MC. Nerve fiber degeneration in the brain in amyotrophic lateral sclerosis. J Neurol Neurosurg Psychiatr 1960; 23: 269–82.

35. Varrone A, Asenbaum S, Vander Borght T, Booij J, Nobili F, Nåigren K, et al. EANM procedure guidelines for PET brain imaging using [18F] FDG, version 2. Eur J Nucl Med Mol Imaging 2009; 36: 2103–10.

36. Verstraete E, van den Heuvel MP, Veldink JH, Blanken N, Mandl RC, Hulshoff Pol HE, et al. Motor network degeneration in amyotrophic lateral sclerosis: a structural and functional connectivity study. PLoS One 2010; 5: e13664.

37. Zimmer ER, Parent MJ, Souza DG, Leuzy A, Lecrux C, Kim HI, et al. [18F] FDG PET signal is driven by astroglial glutamate transport. Nat Neurosci 2017; 20: 393–5.